nature materials

ARTICLES

PUBLISHED ONLINE: 17 AUGUST 2015 | DOI: 10.1038/NMAT4374

Large-area high-quality 2D ultrathin Mo_2C superconducting crystals

Chuan Xu[1†], Libin Wang[2†], Zhibo Liu[1], Long Chen[1], Jingkun Guo[2], Ning Kang[2*], Xiu-Liang Ma[1], Hui-Ming Cheng[1] and Wencai Ren[1*]

Transition metal carbides (TMCs) are a large family of materials with many intriguing properties and applications, and high-quality 2D TMCs are essential for investigating new physics and properties in the 2D limit. However, the 2D TMCs obtained so far are chemically functionalized, defective nanosheets having maximum lateral dimensions of ~10 μm. Here we report the fabrication of large-area high-quality 2D ultrathin α-Mo_2C crystals by chemical vapour deposition (CVD). The crystals are a few nanometres thick, over 100 μm in size, and very stable under ambient conditions. They show 2D characteristics of superconducting transitions that are consistent with Berezinskii–Kosterlitz–Thouless behaviour and show strong anisotropy with magnetic field orientation; moreover, the superconductivity is also strongly dependent on the crystal thickness. Our versatile CVD process allows the fabrication of other high-quality 2D TMC crystals, such as ultrathin WC and TaC crystals, which further expand the large family of 2D materials.

Like graphene[1,2], large-area high-quality two-dimensional (2D) crystals are essential for investigating new physics and properties in the 2D limit, and for many fascinating applications—in particular, electronics and optoelectronics. Transition metal carbides are a large family of materials that combine the properties of ceramics and metals because of the incorporation of carbon atoms into the metal lattice[3,4]. On the one hand, they are very strong and extremely hard, with very high melting points, high stability and good corrosion resistance at high temperatures, good thermal shock resistance and low chemical reactivity[3,4]. On the other hand, they show excellent catalytic activity, comparable to the noble metals commonly used in many reactions[3,4]. Moreover, many TMCs, such as Mo_2C, W_2C, WC, TaC and NbC, exhibit superconductivity[3–7].

Recently, functionalized 2D TMC nanosheets (MXene, with the formula $M_{n+1}C_nT_x$, where M is a transition metal and T_x denotes surface functionalization) have been synthesized by selective etching of the 'A' layer (generally group IIIA and IVA elements) from layered ternary MAX phases, using concentrated hydrofluoric acid or a solution of lithium fluoride and hydrochloric acid[8–12]. They have been theoretically predicted or experimentally demonstrated to have many interesting properties, such as highly efficient thermoelectric conversion and electrochemical energy storage[8–10]. Nevertheless, such chemically derived functionalized 2D TMC sheets are very small, with lateral sizes ranging from hundreds of nanometres to ~10 μm, suffer from severe structural defects, are terminated by hydroxyl and/or other oxygen-containing groups, and have fluorine present on their surface[8–12]. Like other 2D crystals such as graphene, the lack of large-area high-quality 2D TMC crystals has hindered studies of their intrinsic properties.

Here we develop a chemical vapour deposition (CVD) process, with methane as the carbon source and a Cu foil sitting on a Mo foil as the substrate at a temperature above 1,085 °C, to grow high-quality 2D ultrathin α-Mo_2C crystals a few nanometres in thickness with lateral sizes of over 100 μm (see Methods). α-Mo_2C is a typical superconducting TMC (ref. 7), in which Mo atoms are in a slightly distorted hexagonal close-packed (hcp) arrangement, with C atoms occupying ordered positions in the octahedral voids of the Mo lattice, forming an orthorhombic crystal structure[13]. The high growth temperature allows the Cu to melt and a Mo–Cu alloy is formed at the liquid Cu/Mo interface. Subsequently, Mo atoms diffuse from the interface to the surface of the liquid Cu to form Mo_2C crystals by reacting with the carbon atoms from the decomposition of methane. The use of a very low concentration of methane is the key to obtaining ultrathin α-Mo_2C crystals instead of graphene (Supplementary Fig. 1). In addition, rapid cooling after CVD growth is essential to obtain clean ultrathin α-Mo_2C crystals free from Mo nanoparticles on their surface (Supplementary Fig. 2). After CVD growth, the ultrathin α-Mo_2C crystals were transferred to SiO_2/Si substrates or transmission electron microscope (TEM) grids using a mild Cu etchant, $(NH_4)_2S_2O_8$ (see Methods), for detailed structural characterization and electronic transport property measurements, similar to the transfer of CVD-grown graphene[14].

The size and thickness of the 2D α-Mo_2C crystals can be easily tuned by changing the experimental conditions. Their nucleation density increases with growth temperature, and their lateral size increases with growth time (Supplementary Figs 3 and 4). Both low and high growth temperatures can be used to grow ultrathin crystals within a short growth time. We have fabricated ~10 μm-sized ultrathin α-Mo_2C crystals with a uniform thickness of ~3 nm in a growth time of 3 min at a temperature of 1,092 °C (Supplementary Fig. 5). At a low growth temperature, no visible thickness increase is observed with growth time (Supplementary Fig. 3, at 1,086 °C). However, a long growth time at a high growth temperature leads to an increase in the thickness of the crystals (Supplementary Fig. 4, at 1,096 °C). Therefore, we used a low growth temperature and long growth time to fabricate large ultrathin α-Mo_2C crystals. We can also fabricate large and thick α-Mo_2C crystals using a high growth

[1]Shenyang National Laboratory for Materials Science, Institute of Metal Research, Chinese Academy of Sciences, Shenyang 110016, China. [2]Key Laboratory for the Physics and Chemistry of Nanodevices and Department of Electronics, Peking University, Beijing 100871, China. †These authors contributed equally to this work. *e-mail: nkang@pku.edu.cn; wcren@imr.ac.cn

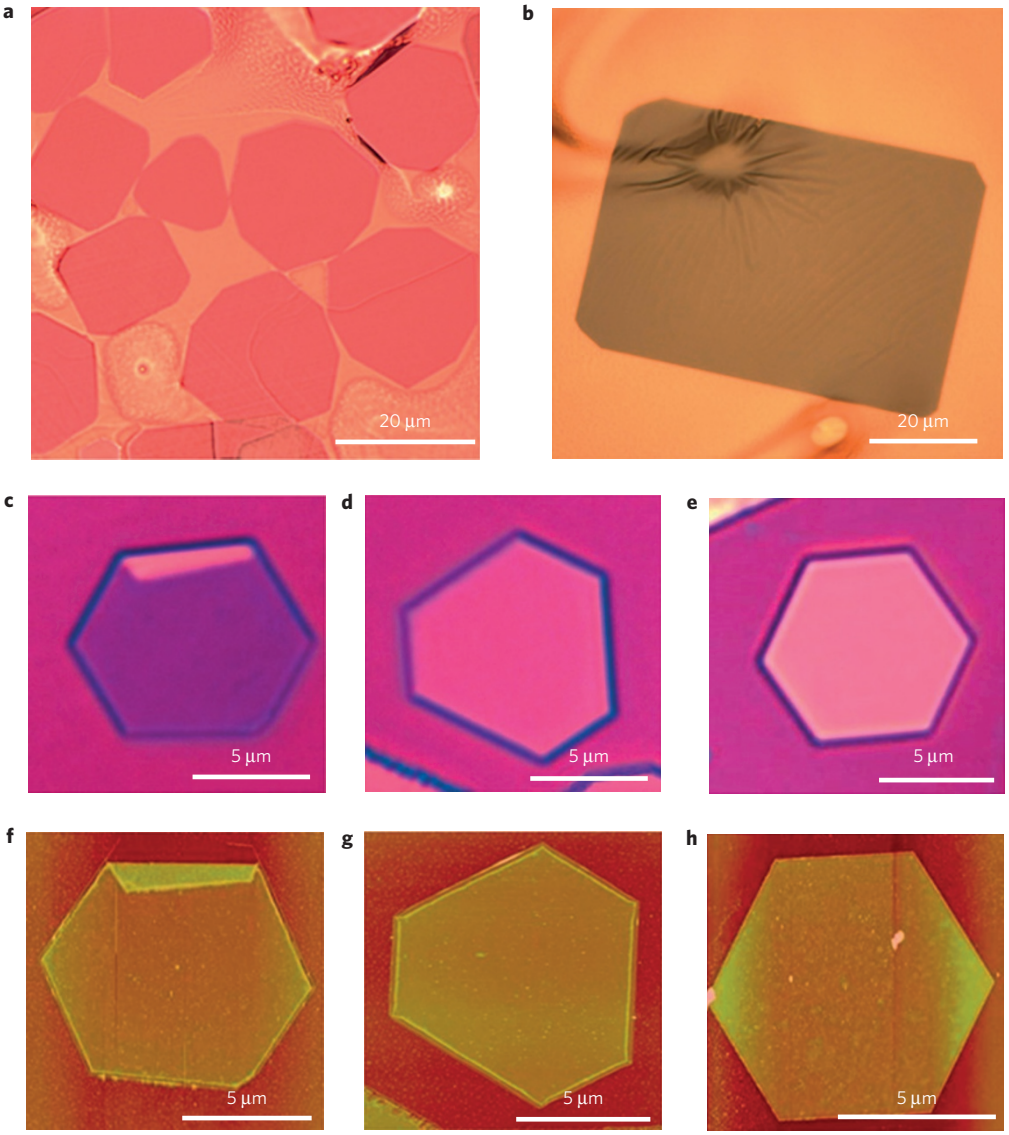

Figure 1 | Large-area 2D ultrathin α-Mo_2C crystals fabricated by CVD. a, Typical optical image of ultrathin α-Mo_2C crystals on a Cu/Mo substrate, showing different regular shapes. **b**, Octagonal ultrathin α-Mo_2C crystal with a size of ~100 μm. **c**–**e**, Optical images of hexagonal ultrathin α-Mo_2C crystals with thicknesses of 6.7 nm (**c**), 8.2 nm (**d**) and 11.2 nm (**e**) transferred onto a 290-nm-thick SiO_2/Si substrate, showing different colours depending on thickness. **f**–**h**, AFM images of the hexagonal ultrathin α-Mo_2C crystals in **c**–**e**, respectively (their height profiles are shown in Supplementary Fig. 7).

temperature and long growth time; however, it is difficult to fabricate individual thick crystals as large as the thinner crystals because of the high nucleation density at a high growth temperature.

Figure 1a shows ultrathin α-Mo_2C crystals fabricated at 1,090 °C with a growth time of 5 min. It is interesting to see that all the ultrathin α-Mo_2C sheets have regular shapes, mainly including triangles, rectangles, hexagons, octagons, nonagons and dodecagons (Fig. 1 and Supplementary Fig. 6), a typical characteristic of well-defined crystals. Most crystals have lateral sizes of ~10 μm and thicknesses of 3–20 nm. With a growth time of 50 min at 1,086 °C, large ultrathin α-Mo_2C crystals with sizes of ~100 μm and thicknesses of mostly less than 10 nm were obtained (Fig. 1b and Supplementary Fig. 3b). Figure 1c–e and f–h, respectively, show typical optical and atomic force microscope (AFM) images of three hexagonal ultrathin α-Mo_2C crystals with thicknesses ranging from ~6 to ~11 nm (Supplementary Fig. 7). It is worth noting that the crystals have a uniform thickness and a smooth surface. Similar to graphene[15], they show different colours on SiO_2/Si substrates under an optical microscope (Fig. 1c–e), which allows rapid thickness identification. Surprisingly, all the ultrathin α-Mo_2C crystals show excellent stability in various liquids, such as water, ethanol, acetone, isopropanol and HCl (Supplementary Fig. 8), under ambient conditions, and show no visible structural change even after thermal annealing in air at 200 °C for 2 h (Supplementary Fig. 9).

We used high-resolution transmission electron microscopy (HRTEM), scanning transmission electron microscopy (STEM), energy dispersive X-ray spectroscopy (EDS) and electron diffraction (ED) to identify the chemical composition, crystal structure and quality of these ultrathin Mo_2C crystals (Fig. 2). Figure 2a shows a low-magnification high-angle annular dark-field (HAADF)-STEM image of a hexagonal 2D Mo_2C crystal. EDS measurements indicate that the crystal is composed of Mo and C with an atomic ratio of ~2:1 (Supplementary Fig. 10). Moreover, Mo and C are uniformly distributed across the whole sheet (Fig. 2b–d), indicating the uniform chemical composition. To identify the structure of the 2D crystal, we tilted the sample at a series of angles and recorded the corresponding zone axis selective area ED (SAED) patterns (Fig. 2e and Supplementary Fig. 11) and convergent beam ED

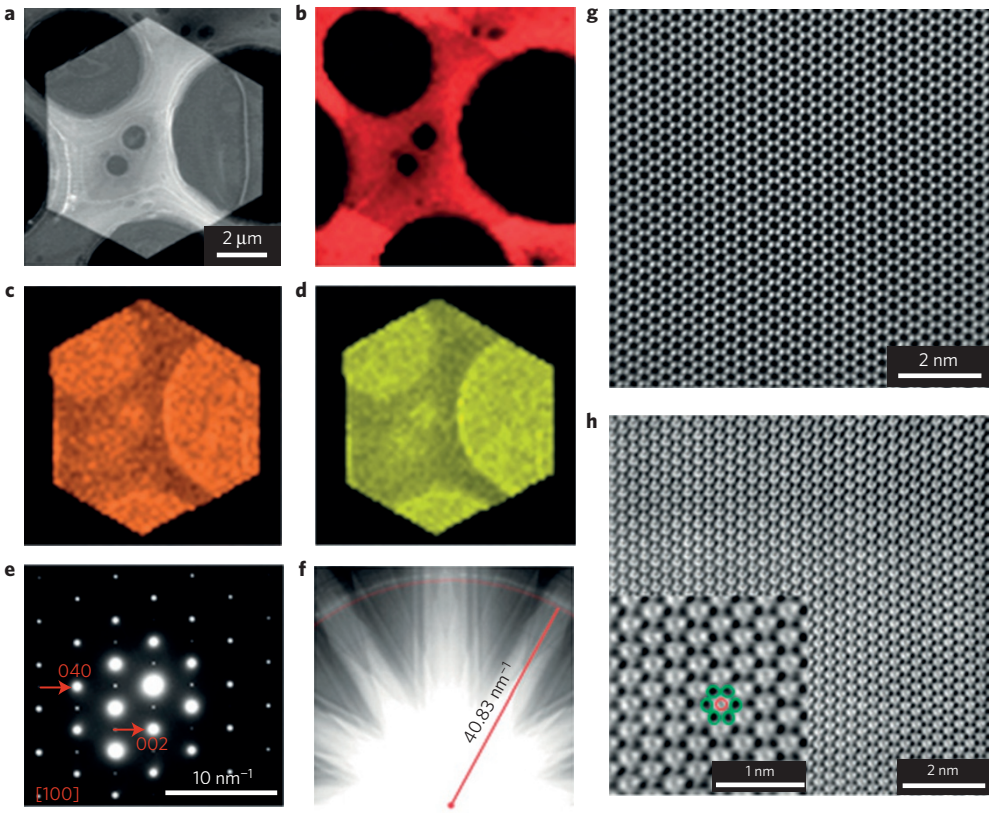

Figure 2 | Characterization of 2D ultrathin α-Mo_2C crystals. a, Low-magnification HAADF-STEM image of a hexagonal 2D α-Mo_2C crystal. **b**–**d**, EDS elemental mapping of C–K (**b**), Mo–K (**c**) and Mo–L (**d**) lines across the sheet in **a**, showing the uniform distribution of C and Mo. **e**, SAED pattern along the [100] zone axis. **f**, CBED pattern along the [100] zone axis, showing the radius of the first-order Laue ring of 40.83 nm^{-1}. **g**,**h**, Atomic-level HAADF-STEM (**g**) and BF-STEM (**h**) images of the α-Mo_2C sheet in **a**. Note that the Mo atoms (white dots in **g**) are arranged in a hcp structure, and the C atoms (black dots indicated by red circle in the inset of **h**) are located at the centre of six Mo atoms (black dots indicated by green circles in the inset of **h**) surrounding it, forming an orthorhombic structure, with no defects, disorders or impurities being observed.

(CBED) patterns (Fig. 2f). Figure 2e shows the SAED pattern along the [100] zone axis. The derived lattice parameters of the crystal from SAED patterns are $b = 5.98$ Å and $c = 5.21$ Å. The lattice parameter a was determined from the CBED pattern (Fig. 2f) to be 4.77 Å according to $r^2 + (\lambda^{-1} - a^{-1})^2 = \lambda^{-2}$, where $\lambda = 0.00251$ nm is the electron wavelength in a 200 kV TEM, and $r = 40.83\ nm^{-1}$ is the radius of the first-order Laue ring. These lattice parameters are consistent with those of orthorhombic Mo_2C (α-Mo_2C; ref. 13). The selective formation of orthorhombic α-Mo_2C is attributed to its higher stability than other molybdenum carbide structures[16].

Figure 2g,h shows typical atomic-level HAADF-STEM and bright-field (BF)-STEM images of ultrathin α-Mo_2C crystals, respectively. It can be found that all the Mo atoms are closely packed into a hexagonal structure (Fig. 2g). Compared with the HAADF-STEM image, which is sensitive only to heavy atoms, the BF-STEM image is sensitive to both light and heavy atoms when the sample becomes very thin. From Fig. 2h, we can clearly see the C and Mo atoms, which form an orthorhombic structure as discussed above, with C atoms located at the centre surrounded by six Mo atoms in the view along the [100] direction. More importantly, no defects, disorders or impurities are observed, even over a large area (Fig. 2g,h, and Supplementary Fig. 12), indicating the very high quality of our ultrathin α-Mo_2C crystals. Similar measurements and analyses of dozens of ultrathin Mo_2C samples with different shapes indicate that all the samples are high-quality α-Mo_2C crystals (Supplementary Fig. 13). Moreover, all these crystals grow along the [100] direction, perpendicular to their surfaces.

These stable high-quality ultrathin α-Mo_2C crystals with different thicknesses provide an ideal system to explore the intrinsic properties of TMCs in the 2D limit. Here we studied their transport properties. Figure 3a shows the temperature dependence of the sheet resistance of a 7.5-nm-thick α-Mo_2C crystal in various magnetic field strengths perpendicular to the crystal plane, with an excitation current of 1 μA. At zero magnetic field, the resistance begins to decrease at 3.6 K and drops to zero at 2.76 K, indicating the onset of superconductivity. With increasing magnetic field, the transition temperature shifts to lower temperatures, and the superconducting transition broadens. A magnetic field of about 1.5 T completely suppresses superconductivity down to the lowest temperature. The superconducting characteristics of ultrathin α-Mo_2C crystals are further confirmed by measuring the differential resistance at zero magnetic field as a function of bias current for different temperatures (Supplementary Fig. 14). Similar superconducting behaviour has been observed in all the measured ultrathin α-Mo_2C crystals with different thicknesses and shapes (Supplementary Fig. 15).

To investigate the dimensionality of the superconductivity in our crystals, we studied the dependence on magnetic field orientation of the superconducting transition. Figure 3b shows the magnetic field dependence of the sheet resistance at selected angles, θ, measured at 1.9 K for a 8.3-nm-thick crystal, where θ denotes the tilt angle between the crystal plane and the magnetic field direction, as depicted in the inset of Fig. 3d. As the magnetic field is tilted towards the crystal plane ($\theta \rightarrow 0$), the transition to superconductivity shifts sharply to higher field. As the 2D limit is approached, it is well known that the upper critical field in a parallel field configuration

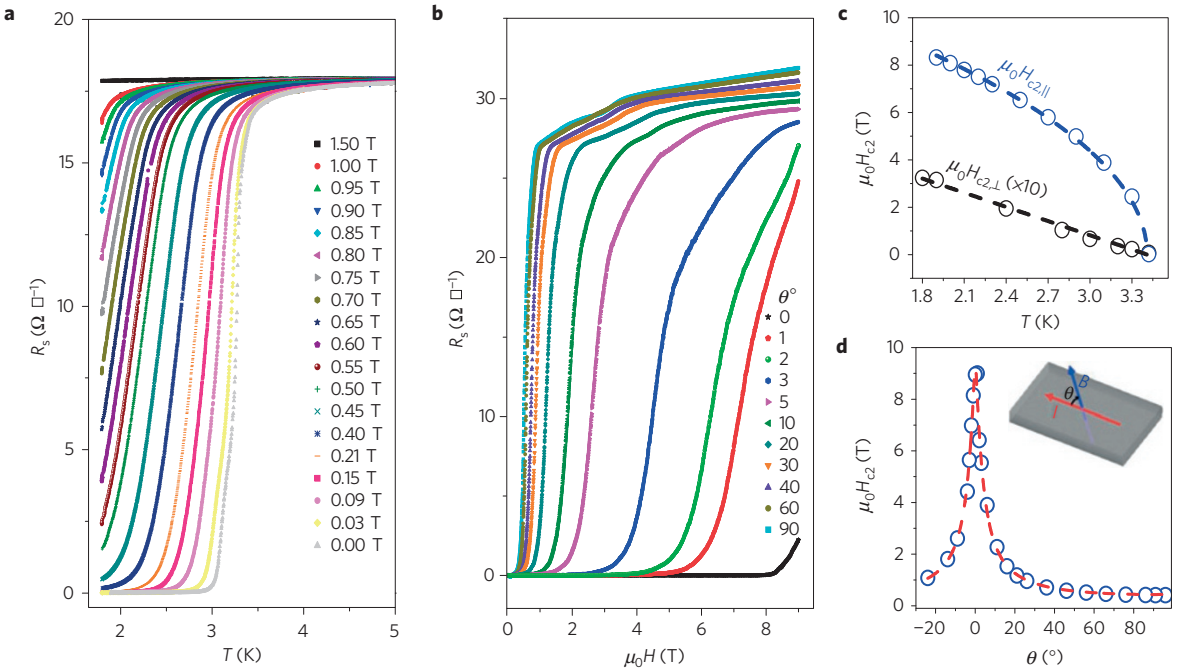

Figure 3 | 2D superconducting characteristics of ultrathin α-Mo_2C crystals. a, Superconducting resistive transition of a 7.5-nm-thick α-Mo_2C crystal for different perpendicular magnetic field strengths. **b**, Magnetic field dependence of the sheet resistance of a 8.3-nm-thick α-Mo_2C crystal, measured with different magnetic field orientations at 1.9 K. The observation of a higher critical field in the parallel field configuration is consistent with the anisotropy of the 2D superconductivity. **c**, Temperature dependence of the upper critical field in directions parallel and perpendicular to the crystal plane, showing strong anisotropy. Dashed lines correspond to theoretical curves obtained from the 2D GL theory. **d**, Upper critical field $H_{c2}(\theta)$ as a function of magnetic field angle θ. The dashed line is a fit to the data following the Tinkham formula for a 2D superconductor. The inset shows the arrangement of the experimental configuration and the definition of the magnetic field direction θ.

is greatly enhanced[17–19]. Therefore, the existence of such strong anisotropy provides direct evidence of the 2D character of the superconductivity for our ultrathin α-Mo_2C crystals.

The temperature dependence of the out-of-plane upper critical field $H_{c2,\perp}$ and in-plane upper critical field $H_{c2,\parallel}$ can be used to extract the value of the coherence length and effective thickness of the 2D superconductor. We define the superconducting critical transition temperature (T_c) under different applied magnetic fields as the temperature at which the sheet resistance drops to 10% of the normal state value just above the onset. Figure 3c shows the temperature-dependent upper critical field in directions parallel and perpendicular to the crystal plane. As for the perpendicular case, $H_{c2,\perp}$ shows a linear behaviour close to T_c, which is consistent with the standard linearized Ginzburg–Landau (GL) theory for superconductors[17]

$$H_{c2,\perp}(T) = \frac{\Phi_0}{2\pi\xi_{GL}(0)^2}\left(1-\frac{T}{T_c}\right)$$

where $\xi_{GL}(0)$ is the zero-temperature GL in-plane coherence length and Φ_0 is the magnetic flux quantum. From the fitting of $H_{c2,\perp}(T)$ data, we can estimate the corresponding coherence length $\xi_{GL}(0) \approx 22.0 \pm 0.4$ nm. The temperature dependence for the parallel field direction follows the behaviour expected for a 2D superconducting film

$$H_{c2,\parallel}(T) = \frac{\Phi_0\sqrt{12}}{2\pi\xi_{GL}(0)d_{SC}}\left(1-\frac{T}{T_c}\right)^{-1/2}$$

where d_{SC} is the superconducting thickness. From the analysis of $H_{c2,\parallel}$, we can extract a value for the superconducting thickness of $d_{SC} \approx 4.1 \pm 0.1$ nm. This value is much smaller than $\xi_{GL}(0)$, which is consistent with the 2D behaviour of the superconductivity.

In Fig. 3d, we show a plot of H_{c2} as a function of θ at 1.9 K, which exhibits a sharp cusp at the maximum when the magnetic field is applied parallel to the crystal plane. The angular dependence of $H_{c2}(\theta)$ can be described well by the known Tinkham formula for a superconductor in the 2D regime ($d_{SC} < \xi$; ref. 17):

$$\left|\frac{H_{c2}(\theta)\sin\theta}{H_{c2,\perp}}\right| + \left(\frac{H_{c2}(\theta)\cos\theta}{H_{c2,\parallel}}\right)^2 = 1$$

The resulting fitting curve is plotted as the dashed line in Fig. 3d, thus further confirming the 2D nature of the superconducting state.

To further understand the superconductivity in ultrathin α-Mo_2C crystals, we carried out current–voltage (I–V) measurements in the superconducting transition region. Figure 4a shows I–V curves taken at temperatures ranging from 1.8 to 3.1 K on a log–log scale. The measured data exhibit a power-law dependence, $V \propto I^{\alpha}$, becoming increasingly nonlinear with decreasing temperature, consistent with expectations for a 2D superconductor based on the theoretical model of the Berezinskii–Kosterlitz–Thouless (BKT) transition[20,21]. Figure 4b shows the temperature dependence of the exponent α. Below T_c, $\alpha(T)$ increases from unity, growing rapidly below 2.8 K. We identify the temperature $T = 2.86$ K at which the exponent α reaches a value of 3 as the BKT transition temperature T_{BKT}. An important additional check on the consistency of the BKT transition can be obtained from the analysis of the temperature-dependent resistance at zero magnetic field. At temperatures just above T_{BKT}, $R(T)$ can be predicted using the following equation[22–24]

$$R = R_0 \exp(-bt^{-1/2}) \quad (1)$$

where R_0 and b are material-specific parameters and $t = T/T_{BKT} - 1$ is the reduced temperature. As shown in Fig. 4c, the temperature-dependent resistance measured can be fitted well with

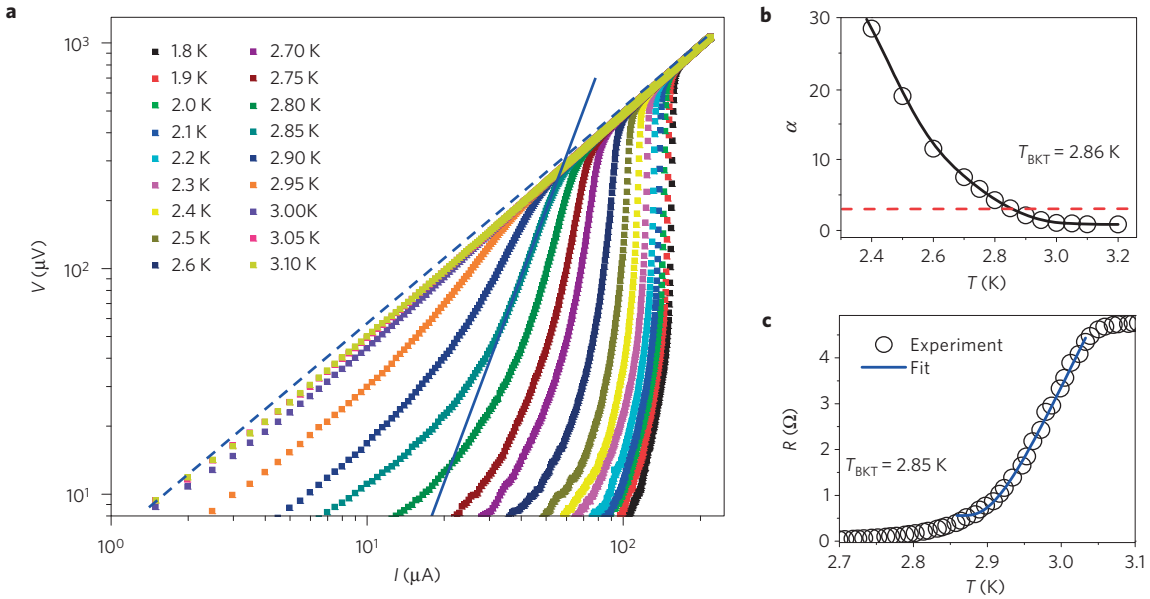

Figure 4 | BKT transition of 2D ultrathin α-Mo_2C crystals. a, V–I characteristic at different temperatures on a logarithmic scale. The dashed blue line indicates the ohmic behaviour expected at high temperature. The solid blue line corresponds to the $V \propto I^3$ behaviour expected at the BKT transition. **b**, Temperature dependence of the exponent α deduced from the power-law behaviour, $V \propto I^{\alpha}$. As indicated by the red dashed line, α approaches 3 at $T = 2.86$ K. **c**, Temperature dependence of the resistance. The blue line is a fit to the expected BKT transition, yielding $T_{BKT} \approx 2.85$ K.

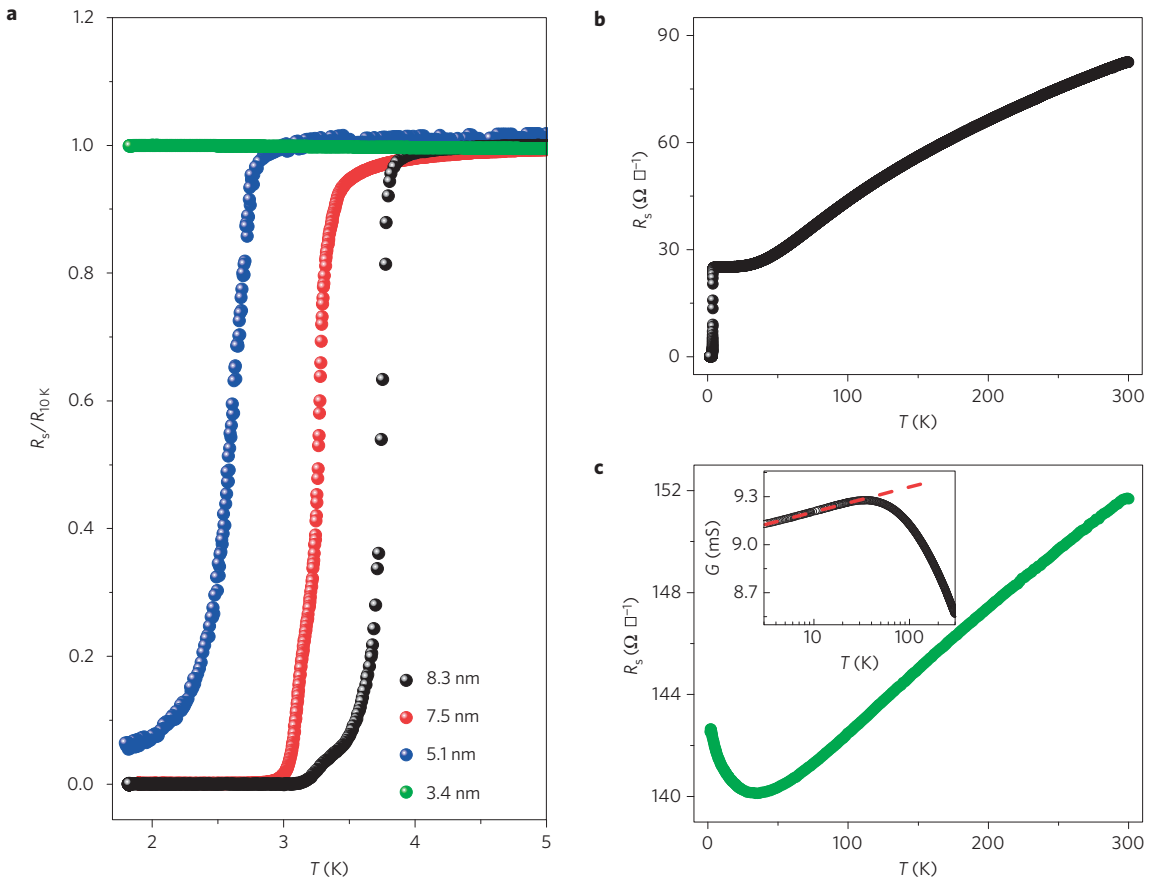

Figure 5 | Thickness dependence of superconductivity of 2D ultrathin α-Mo_2C crystals. a, $R_s(T)$, normalized to the normal state resistance at $T = 10$ K, of α-Mo_2C crystals with thicknesses ranging from 3.4 to 8.3 nm. **b**,**c**, $R_s(T)$ of α-Mo_2C crystals with thicknesses of 8.3 nm (**b**) and 3.4 nm (**c**) at high temperature, showing different behaviours in the normal state. At low temperature, the conductance of the thin crystal exhibits a logarithmic temperature dependence, as indicated by the straight dashed line (inset of **c**), suggesting a 2D weak localization effect.

the BKT model as given in equation (1), yielding $T_{BKT} \approx 2.85$ K, which is in good agreement with the value extracted from the nonlinear $V(I)$ characteristics. This observed feature of the BKT transition provides further strong evidence for the 2D nature of the superconductivity in ultrathin α-Mo_2C crystals.

We then studied the thickness dependence of the superconducting behaviour of the high-quality ultrathin α-Mo_2C crystals. Figure 5a shows the normalized sheet resistance R_s as a function of temperature for thicknesses ranging from 3.4 to 8.3 nm in the superconducting transition regime. It is important to note that our high-quality ultrathin α-Mo_2C crystals show suppression of the superconducting transition as the sheet thickness decreases, providing direct and unambiguous experimental evidence of intrinsic thickness-dependent superconductivity. In a thick α-Mo_2C crystal (8.3 nm thick), the R_s–T curve shows metallic characteristics ($dR/dT > 0$) before the onset of the superconducting transition (Fig. 5b). For the thinnest α-Mo_2C crystal studied (~3.4 nm), the resistance reaches a local minimum at a characteristic temperature T_{min} near 35 K (Fig. 5c). Interestingly, below T_{min}, we observed a negative temperature derivative of R ($dR/dT < 0$), indicating an insulating behaviour in the normal state.

On the basis of Hall measurements (Supplementary Fig. 16), we determined a carrier density of ~$4–5 \times 10^{16}$ cm^{-2} and a mean free path of ~30–40 nm. The corresponding Ioffe-Regel criterion, $k_F l \sim 200–300$, is rather large, where k_F is the 2D Fermi wavevector and l is the mean free path. This implies that strong localization effects are unlikely in our samples. As shown in the inset of Fig. 5c, the thin crystals exhibit a logarithmic temperature dependence of the resistance at low temperature, consistent with 2D quantum corrections due to weak localization[25]. We also observed a negative low-field magnetoresistance at low temperatures (Supplementary Fig. 17), resembling a weak localization effect. Similar localization behaviour has been observed previously in other 2D crystals, including mechanically exfoliated high-quality graphene flakes without ripples in the metallic regime[26] and chemically exfoliated defective single-layer Ti_3C_2 sheets[27]. Such a weak localization effect observed in our high-quality α-Mo_2C crystals can be understood by the unavoidable quantum interference of time-reversal electron trajectories in the diffusive regime.

First, it is worth noting that our ultrathin α-Mo_2C crystals are defect-free according to STEM observations. On the basis of transport measurements (Supplementary Fig. 16), in terms of l (~30–40 nm) and ξ (~13–23 nm), these crystals exceed the superconducting clean limit ($l > \xi$). Second, the superconductivity of the ultrathin α-Mo_2C crystals is highly reproducible and stable in air for a few months thanks to their excellent thermal and chemical stability. Third, our ultrathin α-Mo_2C crystals are fabricated using ambient-pressure CVD, without the requirement of an ultrahigh vacuum, which is different from the commonly used molecular beam epitaxial growth method for the fabrication of high-quality 2D superconducting films. Such stable high-quality clean 2D superconducting crystals provide not only a new platform to study 2D superconductor physics, but also an ideal building block to assemble with other 2D crystals in the construction of hybrid materials[28] or van der Waals heterostructures[29] exhibiting possible unusual properties and new phenomena.

Importantly, the CVD growth method developed is versatile, and can be used as a general strategy for fabricating a broad class of high-quality 2D ultrathin TMC crystals. For example, high-quality ultrathin WC and TaC crystals, which were also stable under ambient conditions, were fabricated using W or Ta foils to replace the Mo foils during the growth process (Supplementary Figs 18 and 19). Further HRTEM and ED measurements indicate that ultrathin WC and TaC crystals, respectively, have a hexagonal structure and cubic structure, and grow along the [0001] and [111] directions perpendicular to their surfaces. Moreover, similar to α-Mo_2C crystals, both ultrathin WC and TaC crystals show very high crystallinity, with no defects or disorder being observed. These high-quality 2D ultrathin TMC crystals add a new class of members to the large family of 2D materials, and provide further possibilities for the investigation of many exciting properties and intriguing applications that are complementary to those of existing 2D crystals such as graphene and atomically thin h-BN, chalcogenides and oxides.

Methods

Methods and any associated references are available in the online version of the paper.

Received 26 February 2015; accepted 1 July 2015; published online 17 August 2015

References

1. Novoselov, K. S. *et al.* Electric field effect in atomically thin carbon films. *Science* **306,** 666–669 (2004).
2. Geim, A. K. Graphene: Status and prospects. *Science* **324,** 1530–1534 (2009).
3. Toth, V. L. E. *Transition Metal Carbides and Nitrides* (Academic Press, 1971).
4. Oyama, S. T. *The Chemistry of Transition Metal Carbides and Nitrides* (Springer, 1996).
5. Matthias, B. T. & Hulm, J. K. A search for new superconducting compounds. *Phys. Rev.* **87,** 799–806 (1952).
6. Willerns, R. H., Buehler, E. & Matthias, B. T. Superconductivity of transition-metal carbides. *Phys. Rev.* **159,** 327–330 (1967).
7. Morton, N. *et al.* Superconductivity of molybdenum and tungsten carbides. *J. Less-Common Met.* **25,** 97–106 (1971).
8. Ghidiu, M., Lukatskaya, M. R., Zhao, M. Q., Gogotsi, Y. & Barsoum, M. W. Conductive two-dimensional titanium carbid "clay" with high volumetric capacitance. *Nature* **516,** 78–81 (2014).
9. Lukatskaya, M. R. *et al.* Cation intercalation and high volumetric capacitance of two-dimensional titanium carbide. *Science* **341,** 1502–1505 (2013).
10. Naguib, M., Mochalin, V. N., Barsoum, M. W. & Gogotsi, Y. MXenes: A new family of two-dimensional materials. *Adv. Mater.* **26,** 992–1005 (2014).
11. Naguib, M. *et al.* Two-dimensional nanocrystals produced by exfoliation of Ti_3AlC_2. *Adv. Mater.* **23,** 4248–4253 (2011).
12. Naguib, M. *et al.* Two-dimensional transition metal carbides. *ACS Nano* **6,** 1322–1331 (2012).
13. Parthé, E. & Sadagopan, V. The structure of dimolybdenum carbide by neutron diffraction technique. *Acta Crystallogr.* **16,** 202–205 (1963).
14. Li, X. *et al.* Large-area synthesis of high-quality and uniform graphene films on copper foils. *Science* **324,** 1312–1314 (2009).
15. Gao, L. B., Ren, W. C., Li, F. & Cheng, H. M. Total color difference for rapid and accurate identification of graphene. *ACS Nano* **2,** 1625–1633 (2008).
16. Hugosson, H. W., Eriksson, O., Jansson, U. & Johansson, B. Phase stabilities and homogeneity ranges in 4*d*-transition-metal carbides: A theoretical study. *Phys. Rev. B* **63,** 134108 (2001).
17. Tinkham, M. *Introduction to Superconductivity* (Dover, 1996).
18. Kozuka, Y. *et al.* Two-dimensional normal-state quantum oscillations in a superconducting heterostructure. *Nature* **462,** 487–490 (2009).
19. Reyren, N. *et al.* Anisotropy of the superconducting transport properties of the $LaAlO_3/SrTiO_3$ interface. *Appl. Phys. Lett.* **94,** 112506 (2009).
20. Reyren, N. *et al.* Superconducting interfaces between insulating oxides. *Science* **317,** 1196–1199 (2007).
21. He, Q. L. *et al.* Two-dimensional superconductivity at the interface of a Bi_2Te_3/FeTe heterostructure. *Nature Commun.* **5,** 4247 (2014).
22. Berezinskii, V. L. Destruction of long-range order in one-dimensional and two-dimensional systems possessing a continuous symmetry group. II. Quantum systems. *Sov. Phys. JETP* **34,** 610–616 (1972).
23. Kosterlitz, J. M. & Thouless, D. J. Ordering, metastability and phase transitions in two-dimensional systems. *J. Phys. C* **6,** 1181–1203 (1973).
24. Halperin, B. I. & Nelson, D. R. Resistive transition in superconducting films. *J. Low Temp. Phys.* **36,** 599–616 (1979).
25. Bergmann, G. Weak localization in thin films. *Phys. Rep.* **107,** 1–58 (1984).
26. Morozov, S. V. *et al.* Strong suppression of weak localization in graphene. *Phys. Rev. Lett.* **97,** 016801 (2006).
27. Halim, J. *et al.* Transparent conductive two-dimensional titanium carbide epitaxial thin films. *Chem. Mater.* **26,** 2374–2381 (2014).
28. Allain, A., Han, Z. & Bouchiat, V. Electrical control of the superconducting-to-insulating transition in graphene-metal hybrids. *Nature Mater.* **11,** 590–594 (2012).
29. Geim, A. K. & Grigorieva, I. V. Van der Waals heterostructures. *Nature* **499,** 419–425 (2013).

Acknowledgements

This work was supported by the National Natural Science Foundation of China (Nos. 51325205, 51290273, 51221264, 51172240 and 11374019), the Ministry of Science and Technology of China (No. 2012AA030303) and the Chinese Academy of Sciences (Nos. KGZD-EW-303-1 and KGZD-EW-T06).

Author contributions

W.R. conceived and supervised the project, and designed the experiments; C.X. and L.C. designed and carried out growth experiments under the supervision of W.R. and H.-M.C.; Z.L. performed TEM measurements and analyses under the supervision of X.-L.M.; L.W. and J.G. carried out transport measurements under the supervision of N.K.; W.R. and N.K. analysed data and wrote the manuscript. All the authors discussed the results and commented on the manuscript.

Additional information

Supplementary information is available in the online version of the paper. Reprints and permissions information is available online at www.nature.com/reprints. Correspondence and requests for materials should be addressed to W.R. or N.K.

Competing financial interests

The authors declare no competing financial interests.

Methods

CVD growth and transfer of ultrathin α-Mo_2C crystals. A Cu foil (Alfa Aesar, 99.5% purity, 10 μm thick) was cut into 5 × 5 mm^2 pieces and placed on top of a Mo foil (Alfa Aesar, 99.95% purity, 100 μm thick) of the same size. They were then placed in a quartz tube of outer diameter 25 mm and inner diameter 22 mm to act as the growth substrates for ultrathin α-Mo_2C crystals. Subsequently, the Cu/Mo bilayer substrates were heated above 1,085 °C in a horizontal tube furnace (Lindberg Blue M, TF55030C) under H_2 (200 sccm). A small amount of CH_4 (0.35 sccm) was then introduced into the reaction tube at ambient pressure to initiate the growth of 2D α-Mo_2C crystals. The growth usually lasted 2–50 min. The longer the growth time, the larger the size of the ultrathin α-Mo_2C crystals. To grow ultrathin WC or TaC crystals, W or Ta foils were used to replace the Mo foil in the above process. After the reaction, the samples were quickly removed from the high-temperature zone under H_2, to ensure rapid cooling of the samples to room temperature.

The transfer of ultrathin α-Mo_2C crystals is similar to the transfer of graphene[25]. A thin layer of poly (methyl methacrylate) (PMMA, weight-averaged molecular mass M_w = 600,000, 4 wt% in ethyl lactate) was first spin-coated on the surface of ultrathin α-Mo_2C crystals at 5,000 r.p.m. for 1 min and cured at 180 °C for 30 min; the PMMA-coated samples were then immersed in a 0.2 M $(NH_4)_2S_2O_8$ solution at 70 °C for 10 min to etch the Cu substrate. After that, the PMMA-coated ultrathin α-Mo_2C crystals were stamped onto target substrates, such as SiO_2/Si and TEM grids, and warm acetone (55 °C) was used to dissolve the PMMA layer and obtain clean ultrathin α-Mo_2C crystals.

Structural characterization. The morphology of the ultrathin α-Mo_2C crystals was identified by optical microscopy (Nikon LV 100D), the thickness by AFM (Nanoscope IIIa), and the chemical composition, crystalline quality and detailed crystal structure by TEM (FEI Tecnai T12, 120 kV for dark-field TEM imaging and SAED measurements; JEOL JEM 2100, 200 kV for CBED measurements; FEI Tecnai F20, 200 kV for HRTEM observations; FEI Tecnai F30, 300 kV for STEM and EDS measurements). We used the same method and equipment to characterize the morphology, crystalline quality and detailed crystal structure of the ultrathin WC and TaC crystals. Atomic-level HAADF-STEM and BF-STEM images, shown in Fig. 2g,h and Supplementary Fig. 12, were obtained from a 300 kV STEM (FEI Titan3 G2 60-300) equipped with a high-brightness field-emission gun (X-FEG), double spherical aberration corrector and a monochromator. The probe convergence angle is 21.4 mrad and the camera length is 185 mm.

Device fabrication and transport measurements. The ultrathin α-Mo_2C crystals used here were 10–20 μm in lateral size. Individual samples on 290-nm-thick SiO_2/Si substrates were first located using a scanning electron microscope, then electrodes consisting of Ti/Au (5/90 nm) were formed directly on the top surface by electron-beam lithography, followed by electron-beam evaporation. The source–drain separations of devices varied between 0.5 and 2 μm. The transport measurements were performed in a standard four-terminal configuration from room temperature to 1.8 K with a Quantum Design Dynacool Physical Properties Measurement System. The resistance was measured using the standard low-frequency lock-in technique with a drive current of 0.1–100 μA. The magnetic field was always applied perpendicular to the ultrathin α-Mo_2C crystal plane, except for the angular-dependence measurements of the anisotropic superconducting transition.